Processing Conditions Effect on Dispersion Evolution in a Twin-Screw Extruder: Polypropylene-Clay Nanocomposites

Joana M. Barbas, Ana V. Machado, José A. Covas

University of Minho, Institute of Polymers and Composites (IPC) and I3N, Guimarães, Portugal.

Abstract

Polymer-clay nanocomposites are often manufactured using twin-screw extruders. Processing conditions, namely screw speed and feed rate, are known to strongly influence the final dispersion levels attained. The effect of these parameters on the evolution of dispersion along the extruder for a system consisting of polypropylene, polypropylene grafted with maleic anhydride, and an organoclay is investigated. Inline near-infrared measurements were performed at various axial locations plus die outlet. At the same positions, local average mass temperature and minimum residence time were also monitored. In addition, samples were quickly removed from the extruder for subsequent offline characterization. Regardless of the processing conditions, dispersion develops rapidly upon melting, with a much slower pace downstream.

Keywords: Dispersion, Nanocomposites, Near-infrared spectroscopy, Twin-screw extrusion

Introduction

Direct melt intercalation is currently the favored route to prepare polymer-clay nanocomposites, due to the significant dispersion levels attained, adaptability to the characteristics of the materials being processed, continuous production, and suitability for industrial manufacture [1-3]. The properties of the ingredients and mutual chemical

affinity [4-7], the type of equipment [1,2], and the processing conditions [3,8 – 10] influence evolution [3,9,11] and final dispersion levels [12-16]. When using twin-screw compounding, it is generally acknowledged that high screw speeds promote better dispersion due to the greater hydrodynamic stresses induced by the shear rates [1 – 3,9,11 – 14]. However, opposing results have also been reported [8, 15, 16]. Low feed rates improve exfoliation owing to the corresponding increase of residence time [2,3,9,14]. In turn, high processing temperatures are often detrimental for dispersion, as they induce degradation of the clay surfactant and, eventually, of the polymer matrix [1,2,16]. The effect of processing conditions on the evolution of dispersion along the extruder axis is much less known [3,9,11,17]. The balance between local time for diffusion of

the polymer chains inside the clay galleries and stress for delamination of the clay stacks is much more difficult to predict. Lin et al. [11] studied a polyamide 66/clay composite and reported that after the initial breakdown of the clay agglomerates further shear did not significantly affect subsequent peeling-off of the platelets, which made them conclude that dispersion is mostly governed by the chemical affinity between organoclay and polymer matrix. Lertwimolnun and Vergnes [3, 9] characterized post-mortem samples collected from various locations along the screw of a system consisting of polypropylene (PP), polypropylene grafted with maleic anhydride (PP-g-MA), and an organoclay. They established that dispersion reaches relatively high levels immediately after melting and that processing conditions have a minor impact on intercalation, but strongly influence exfoliation. Depending on processing conditions and screw design, the composite structure could progress, remain constant, or revert along the screw length, the latter being attributed to matrix degradation, although no experimental confirmation was obtained.

Barbas et al. [17] used online rheometry, inline near-infrared (NIR) spectroscopy, medium infrared spectroscopy (Fourier transform infrared, FT-IR), X-ray diffraction (XRD), and electron microscopy (scanning transmitted electron microscopy, STEM) to monitor the evolution of dispersion of an analogous polymer system. Evidence of reversion of intercalation was observed under certain conditions and correlated with degradation of the organoclay surfactant and subsequent degradation of the PP/PP-g-MA matrix. In fact, it has been demonstrated that unsaturated olefins formed by degradation of the alkyl tails of the surfactant can readily react with oxygen to form peroxide species, eventually causing chain scission of the polymer matrix [16, 18, 19]. According to Shah and Paul [16], these degradation effects are maximized during extrusion due to the solubility of the small-chain a-olefins in the polyolefin matrix, accelerating the degradation reaction relatively to what is measured by regular thermogravimetric analysis.

The effect of screw speed (N) and feed rate (Q) on the evolution of dispersion along the extruder of the same PP/PP-gMA/organoclay system is investigated. Inline NIR measurements were performed at various locations along the extruder plus die outlet. At the same positions, local mass temperature and residence time were also monitored, and material was quickly removed from the extruder for offline characterization by rheometry, XRD, FT-IR, and STEM. Regardless of the processing conditions, dispersion develops rapidly, often reaching a maximum in the first mixing zone; a marked decline may occur along the second half of the extruder, as a result of the thermomechanical experience imparted to the material.

Experimental

Materials and Compounding

The constituents of the nanocomposite are identified in Tab. 1. As in the previous study [17], the PP/PP-g-MA/D67G formulation was kept at 90/5/5 wt %. The organoclay was dried overnight in a vacuum oven at 80°C. The nanocomposite was manufactured in a Leistritz LSM 30.34 co-rotating intermeshing twin-screw extruder with the screw profile presented in Fig. 1 which contains a first mixing zone comprising five kneading disks staggered at 90°, four kneading disks staggered at −60°, and a left-handed element, as well as a shorter second mixing zone consisting of six kneading disks staggered at 90°. In a first set of experiments, the feed rate (Q) was set at 3 kg h^{-1} by a Moretto DVM18-L dosing system and the screw speed (N) was varied between 50 and 300 rpm . Then the screw speed was kept constant at 100 rpm and different feed rates (1.5, 3, 6, and 9 kg h^{-1}) were applied. The barrel and die set temperatures were maintained at 200°C in all runs.

Inline Monitoring

An NIR diffuse reflectance probe from Hellma Analytics, fitted with a Dynisco-type thread, was directly fixed to the extruder at L/D = 10,11,19,29, and die (see Fig. 1), where L is the axial length and D is the diameter. The probe has a sapphire window with an illuminated area of approximately 3 mm^2 and a field depth of 3 mm and contacts directly the melt stream. Connection with the NIR spectrometer (Matrix F, Bruker Optics) is made by a fiber optic cable; see detailed description and validation of the experimental methodology in [20,21]. NIR spectra were measured in the range of 12000 − 4500 cm^{-1} with a resolution of 8 cm^{-1} and accumulation of four scans, the acquisition time for each spectrum being approximately 2 s . For each position, a total of 50 spectra were measured at regular intervals during the extrusion runs. Usually, dispersion causes a vertical shift upwards of the baseline, due to the presence of a larger number of smaller particles (clay stacks and/or individual platelets) or of a higher inter-lamellar distance which enhance light-scattering effects. A quantitative relationship can be obtained by relating via chemometrics the spectral differences with the values of reference parameters quantifying dispersion. This is very interesting for practical compounding

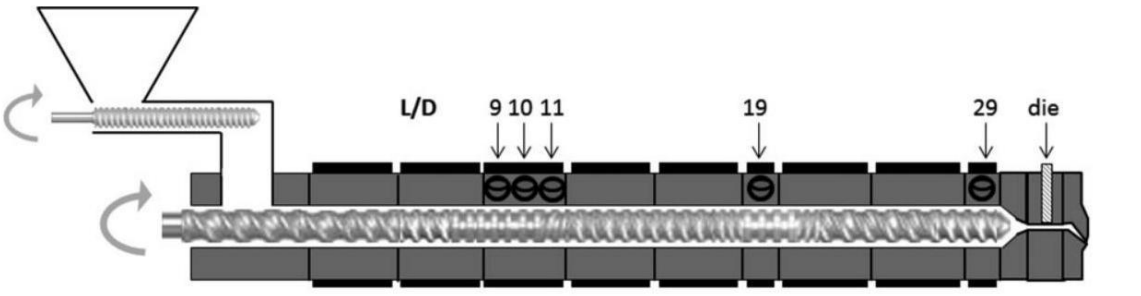

Figure 1. Layout of the twin-screw extruder and identification of the screw profile from feed to tip.

Table 1. Materials used in the work.

Material	Acronym	Producer	Grade	MFI/lamellar distance (CEC; wt % surfactant)
Polypropylene	PP	Lyondell Basell	Moplen HP500N	12 g per 10 min (230°C/2.16 kg)
Compatibilizer	PP-g-MA	Crompton	Polybond 3200 (1 wt % MA)	115 g per 10 min (190°C/2.16 kg)
Montmorillonite clay	D67G	Laviosa	Dellite 67G	3.70 nm (115 meq per 100 g ; 48wt%) [12]

and processing, since the availability of a quick characterization technique, able to estimate the state of dispersion of a given nanocomposite, would enable valuable decisions on the eventual need of corrective actions in terms of material formulation, operating conditions, or even equipment configuration. Because dispersion presents various aspects at different length scales, the model employed here includes seven parameters extracted from oscillatory rheometry (G', G'', σ_0, b; see definitions below), FT-IR (wavenumber shift of the peaks at 1050 and 1080 cm^{-1}), and the specific mechanical energy (SME), a process-related thermomechanical index (mechanical energy input per unit throughput). The model was developed for the same system and process layout based on samples with variable clay loading, compatibilizer content, and screw speed, processed under different feed rates [21].

Material samples were removed from the screw channel at the L/D locations identified in Fig. 1 by means of specially designed sample collecting devices [22]. At $L/D = 10$, melting was still incomplete for the extrusion runs performed at the highest screw speed (300 rpm) and the highest feed rates (6 and 9 kg h^{-1}). Sticking a fast response thermocouple into the melt sample just taken from the extruder provided a good estimate of the local average mass temperature. Moreover, an appraisal of the local minimum residence time could be made by counting the time elapsed between feeding a pigment tracer into the screws and identifying the beginning of a color change in the melt stream.

Offline Characterization

Rotational Rheometry (AR-G2, TA Instruments)

Isothermal (at 200°C) frequency sweeps from 0.1 to 100rads^{-1} were performed using parallel plates with a diameter of 25 mm and a 1 – mm gap, under constant strain (1% for the matrix and 0.5% for the composites). The disks were produced by compression molding at the same temperature, under 20 t during 3 min. Previously [17], online oscillatory rheometry was used to measure the evolution of the rheological response of polymer-organoclay nanocomposites along the extruder. A good match was then found with equivalent offline data which can be interpreted as evidence that the thermal cycles associated to sample preparation and testing have limited impact on the final morphology.

XRD (AXS Nanostar-D8 Discover, Bruker)

Diffraction patterns were obtained using a diffractometer equipped with a CuKa generator ($\lambda = 1.5404$Å) at 40 kV and 40 mA , in a 2θ range between 0.08° and 10°. The organoclay was analyzed directly ($\theta = 2.40°, d_{001} = 3.68$ nm), while the nanocomposite samples were previously compression-molded into disks with a diameter of 20 mm and a thickness of 4 mm .

Electron Microscopy (NanoSEM Nova 200, FEI)

Scanning transmitted electron microscopy (STEM) observations of the composites were performed using an acceleration voltage of 15 kV . Ultrathin sections roughly 80 nm thick were cut from samples under cryogenic conditions ($-60°C$), applying a UC6 ultramicrotome (Leica) equipped with a diamond knife.

Medium FT-IR (FTIR4100, Jasco)

The analysis was performed in transmission mode, in the $4000 - 500$ cm^{-1} interval, with a resolution of 4 cm^{-1} and utilizing 32 scans. The organoclay was investigated with a KBr mortar. The nanocomposite samples were compression-moulded at $200°C$ into films approximately 75μ m thick; three films per sample were analyzed. Wavenumber accuracy and repeatability were checked prior to measurements according to the procedure described in [21]. The region between 1300 and 750 cm^{-1} was fitted with the Pearson VII expression utilizing the Origin ® Pro8 software as described in [21] for the determination of the wavenumber shift at 1050 cm^{-1} (Si-O in-plane) and 1080 cm^{-1} (Si-O out-of-plane) peaks [23,24].

Thermal Gravimetry (Q500, TA Instruments)

Isothermal tests (at various temperatures) during 10 min under a constant flow of nitrogen (60 mL min^{-1}) were carried out with the organoclay (D67G) and polymer matrix (95%PP/ 5% PP-g-MA).

Results and Discussion

Global Effects

It is difficult to unequivocally quantify dispersion and discriminate between intercalation and exfoliation in a polymer/clay nanocomposite. Transmission electron microscopy is capable of providing the adequate magnifications, but since only a small area is analyzed, it remains cumbersome and time-consuming to characterize a representative material sample. Consequently, correlations between the values of material properties or characteristics that can be obtained swiftly, and dispersion levels are of great practical interest and have been the focus of abundant research. A few rheological parameters have been linked to dispersion. An increase of the storage modulus (G') at low frequency, often due to the formation of a plateau, is usually interpreted as evidence of greater dispersion [5, 9, 13, 25-28]. It has also been suggested that the exponent of a power law fitted to the variation of complex viscosity (η^*) with frequency increases with dispersion [25,26]. The rise in melt yield stress (σ_0) was related to an intensification of clay exfoliation [3,9,13]. XRD data presents a region of interest at low 2θ angles due to the diffraction peak of the organoclay, from which the clay interlayer spacing (d_{001}) may be estimated using Bragg's

law [1,3-5]. Typically, the peak center position shifts to lower angles, as the interlayer distance increases due to intercalation of the polymer melt. Fig. 2 presents the effects of screw speed and feed rate on the final dispersion attained, either at the die or die outlet depending on the experimental procedure, as determined by the above techniques and by inline NIR.

To determine σ_0, a modified Carreau-Yasuda model with yield stress was fitted to the experimental complex viscosity curve [3]:

$$|\eta^*(\omega)| = \frac{\sigma_0}{\omega} + \eta_0[1 + \tau\omega^{\mathrm{a}}]^{(\mathrm{b}-1)/\mathrm{a}} \quad (1)$$

where ω is the frequency, τ is the relaxation time, and a and b are the fitting parameters. Although dispersion is expected to be favored by high screw speeds and low feed rates, Fig. 2 suggests that for this polymer/clay system an optimum set of processing conditions maximizes dispersion. Indeed, dispersion improves with increasing screw speed up to 200 rpm , while feed rates higher than 3 kg h^{-1} are detrimental. On a similar track, Kim et al. [29] concluded that dispersion should improve with increasing specific energy input until a critical value is attained. Also, while organoclay D67G presents an initial interlayer spacing of approximately 3.70 nm (Tab. 1), the extrudates exhibit lower spacing which seems unexpected.

Tab. 2 presents the values of process parameters registered during the compounding runs, namely mass temperature and minimum residence time at several axial locations, and total specific mechanical energy (SME). Values lower than 200°C at $L/D = 29$ are unexpected and are probably due to limitations of the barrel control system. At $L/D = 9$, the most upstream monitoring location, melting was not completed. Increasing screw speeds promote faster melt temperature buildup and a higher melt temperature at the die exit. Increasing screw speed from 50 to 200 rpm raised the melt temperature at $L/D = 11$ from 189°C to 217°C, a change of 28°C, and at the die exit from 208°C to 226°C, a rise of 18°C.

As expected, the residence time the molten material was exposed to hydrodynamic stresses (measured by the difference between minimum residence time at die exit and minimum residence time at $L/D = 11$) remained essentially constant. Conversely, an increase in feed rate prompts a small upsurge of mass temperature. Increasing feed rate from 1.5 to 9 kg h^{-1} reduced the melt temperature at $L/D = 11$ from 205°C to 188°C, a difference of 17°C, while at the screw tips and die exit an increase of roughly 3°C was measured, but an important reduction of the residence time from 35 to 14 s at $L/D = 11$ and from 240 to 75 s at the die exit. These results seem to indicate that sufficiently

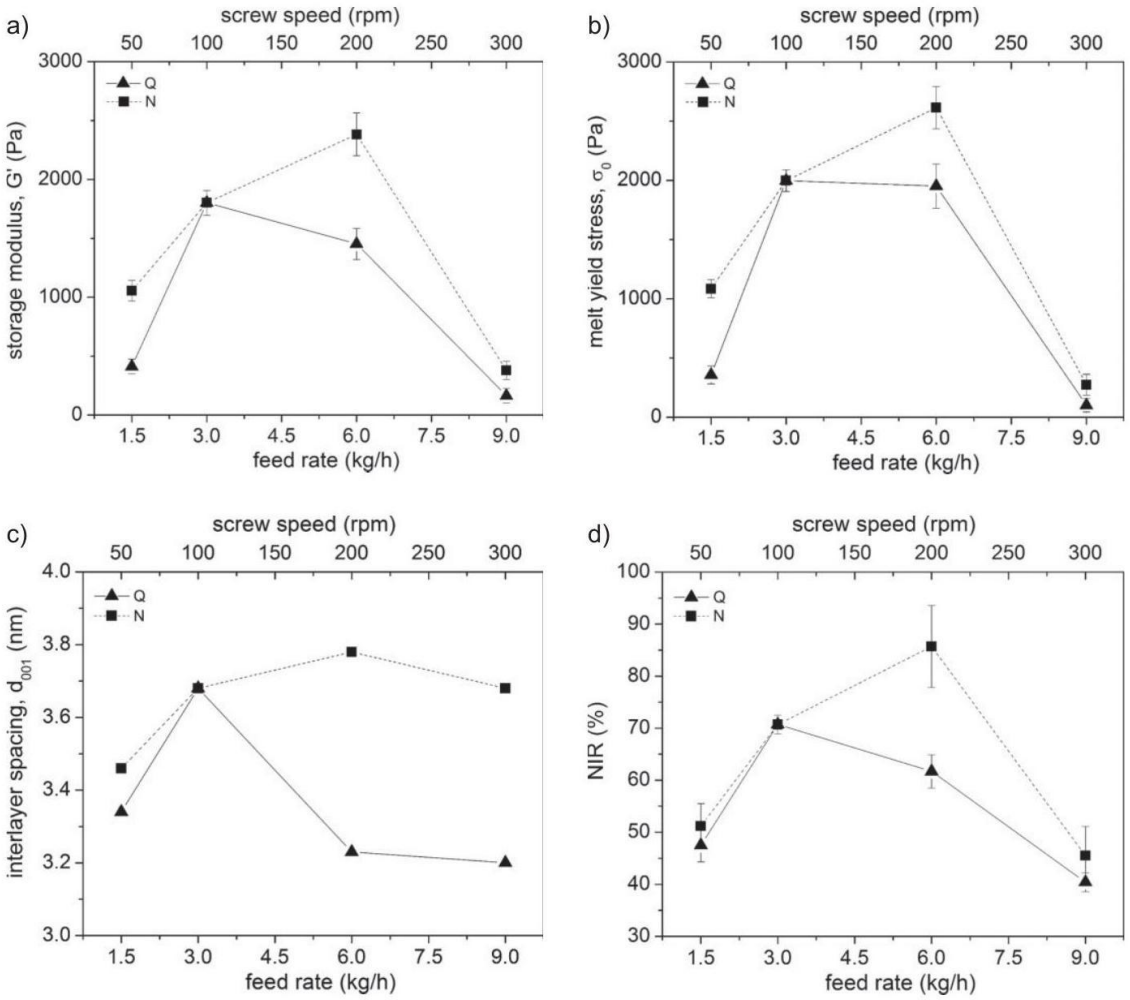

Figure 2. Effect of feed rate and screw speed on final dispersion levels of PP/clay nanocomposites, as assessed by (a) storage modulus (G') measured at 0.1rads^{-1}, (b) melt yield stress (σ_0), (c) interlayer spacing (d_{001}), and (d) NIR.

Table 2. Process parameters registered during the compounding runs.

N [rpm]	Q [kgh^{-1}]	Melt temperature (± SD) [°C]				Residence time (± SD) [s]		SME [kWht^{-1}]
		L/D = 11	L/D = 19	L/D = 29	Die	L/D = 11	Die	
50		188.9(±2	197.5(±0	198.5(±0	207.7(±0	33.3(±1.	142.3(±2	1060
100		198.2(±1	204.9(±0	198.9(±0	207.9(±0	27.0(±2.	138.0(±3	1130
200	3	214.3(±0	216.5(±2	202.0(±0	215.6(±0	15.7(±3.	129.0(±3	1230

300		217.4(±1	232.5(±2	207.4(±1	226.0(±2	10.0(±1.	121.0(±1	1270
	1.5	205.5(±0	208.9(±0	195.0(±0	209.7(±0	34.7(±1.	240.3(±1	1730
100	6	193.1(±1	204.2(±1	198.1(±0	210.8(±0	17.3(±0.	93.3(±1.5	720
	9	187.7(±3	203.4(±0	198.4(±0	213.6(±0	13.7(±1.	74.7(±2.5	570

high screw speeds may cause significant viscous dissipation which, in turn, could decrease matrix viscosity and facilitate its draining out from the clay galleries, or even origin degradation of the organoclay surfactant and subsequent degradation of the PP/PP-g-MA matrix, as detected earlier [17]. An increase in feed rate will probably not significantly affect the level of the hydrodynamic stresses acting on the polymer system, but will strongly reduce their exerting time, thus disturbing dispersion [10, 30]. These hypotheses will be better verified, or otherwise, when studying the evolution of dispersion along the screw axis.

Effect of Screw Speed on the Evolution of Dispersion

Fig. 3 displays the effect of screw speed on the evolution of dispersion along the extruder axis, as determined by inline NIR and rheometry (melt yield stress, σ_0). Since the matrix was not melted at $L/D = 9$, inline NIR measurements started at $L/D = 10$, where the process appeared mostly completed. As seen in Fig. 3 a , according with NIR predictions, at $L/D = 10$ dispersion levels are already significant (between 37% and 89%, de-

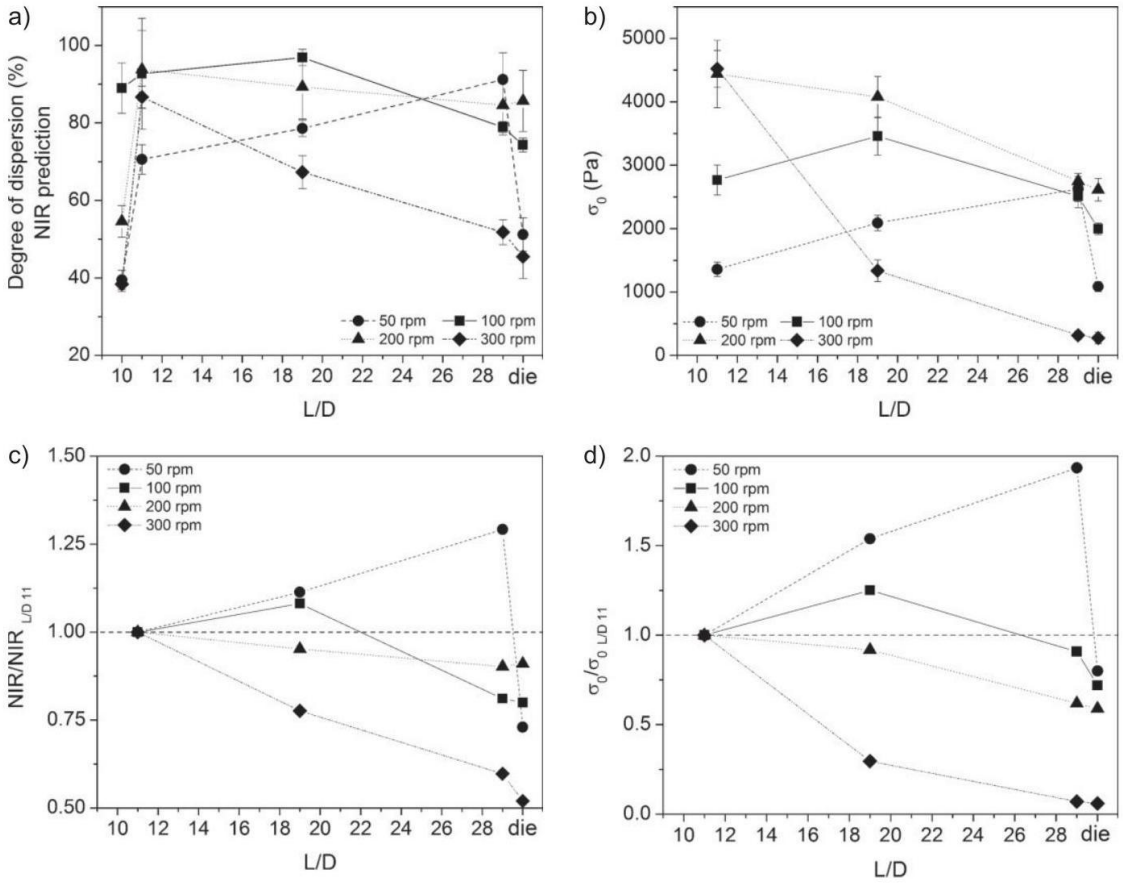

Figure 3. Effect of screw speed on the evolution of dispersion along the extruder axis of PP/clay nanocomposites, as determined by: (a) inline NIR, (b) melt yield stress; (c) and (d) show same data normalized to the values measured at $L/D = 11$. pending on screw speed) and increase sharply until $L/D = 11$ (to 70% and 93%, respectively). This means that dispersion evolved rather quickly, simultaneously with matrix melting, due to the high stresses and deformations generated by the restrictive screw elements. This behavior has obvious similarities to the evolution of morphology and chemical conversion during in situ compatibilization of polymer blends, which also revealed high developing rates in the melting stage [31]. From $L/D = 11$ onwards, the rate of dispersion changes significantly. Except for the lowest screw speed, a plateau or a decrease is predicted, the latter being especially noticeable along the die. The rheological measurements presented in Fig. 3b were performed only at $L/D = 11$ and beyond, as the presence of a molten matrix was indispensable for a proper interpretation of the results. They show the same trend of the NIR data, i.e., a constant value or a decrease of dispersion along the second part of the extruder, except for the composite prepared at 50 rpm and a reduction along the die.

Interestingly, at $L/D = 11$ melt yield stress increases with screw speed, i.e., exfoliation is promoted, according to previously proposed correlations. On the other hand, at the same location the relative degrees of dispersion given by NIR data are the same as the final ones depicted in Fig. 2 d . The data of Figs. 3 a and b was normalized to the value measured at $L/D = 11$, giving rise to Figs. 3 c and d. Within experimental accuracy, these two representations prove that, once melting of the matrix is accomplished, the rate of dispersion evolution along the screw axis decreases with increasing shear rate, i.e., at low

screw speed dispersion progresses axially, at intermediate speeds little changes take place, at high screw speed reversion apparently occurs. Also, flow along the die has a negative impact on dispersion. The global influence of screw speed on dispersion seems to result from the combined effect of evolution prior to $L/D = 11$, upon melting, and beyond $L/D = 11$. This evolution of dispersion inferred from rheological and NIR data is globally confirmed by other dispersion assessment techniques.

Fig. 4 indicates the downstream progression of the XRD patterns for the nanocomposite prepared at 100 rpm and $3\ \mathrm{kg\,h^{-1}}$, for which the above data showed an increase of dispersion until $L/D = 19$, followed by a reversion. A clear shift of the diffraction peak to lower angles can be observed until $L/D = 11$, indicating growing of the interlamellar distance (intercalation). At $L/D = 19$, the broad peak suggests a transition state with the co-existence of intercalated clays and exfoliated clay platelets. From $L/D = 19$ onwards, the peaks shift to higher angles, suggesting a decrease of the interlayer spacing.

The STEM micrographs in Fig. 5 refer to the same nanocomposite. Up to $L/D = 19$, the amount and thickness of intercalated tactoids decrease, revealing a development in both intercalation and exfoliation. Further downstream the opposite develops, with evidence of

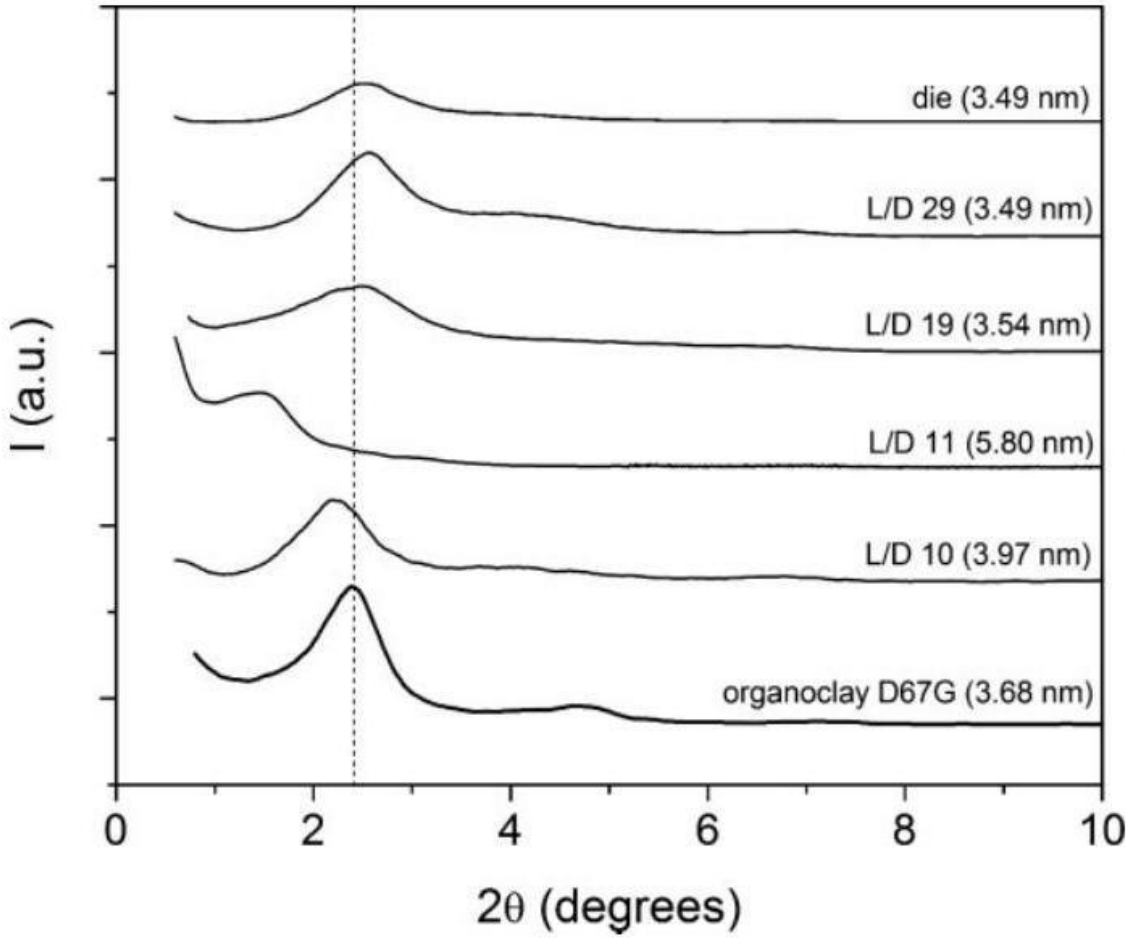

Figure 4. Evolution along the extruder axis of XRD diffraction patterns of PP/clay nanocomposites prepared at 100 rpm and $3\ \mathrm{kg\,h^{-1}}$.

thicker tactoids at the die associated to collapsed platelets. Contrarily, FT-IR spectra of the various available samples did not produce any significant variations, either in terms of the shift of the in-plane peak of the clay at 1050 cm^{-1} to lower wavenumbers, or of the shift of the out-of-plane peak at 1080 cm^{-1} to higher wavenumbers.

Fig. 6 a demonstrates the evolution of average mass temperature from $L/D = 11$ until die exit. The data is presented numerically in Tab. 2. The influence of screw speed on viscous dissipation during flow along the two mixing zones (measurements at $L/D = 11$ and $L/D = 19$, respectively) and die is substantial. At $L/D = 19$, the difference between set and average melt temperature exceeds 30°C. Although temperature relaxes all through the conveying section upstream of the die, the latter causes again an important temperature upsurge, then can reach over 25°C above the set value. Since the thermal stability of clay surfactants is often limited [16,18,19], D67G was subjected to TGA isothermal tests at various temperatures.

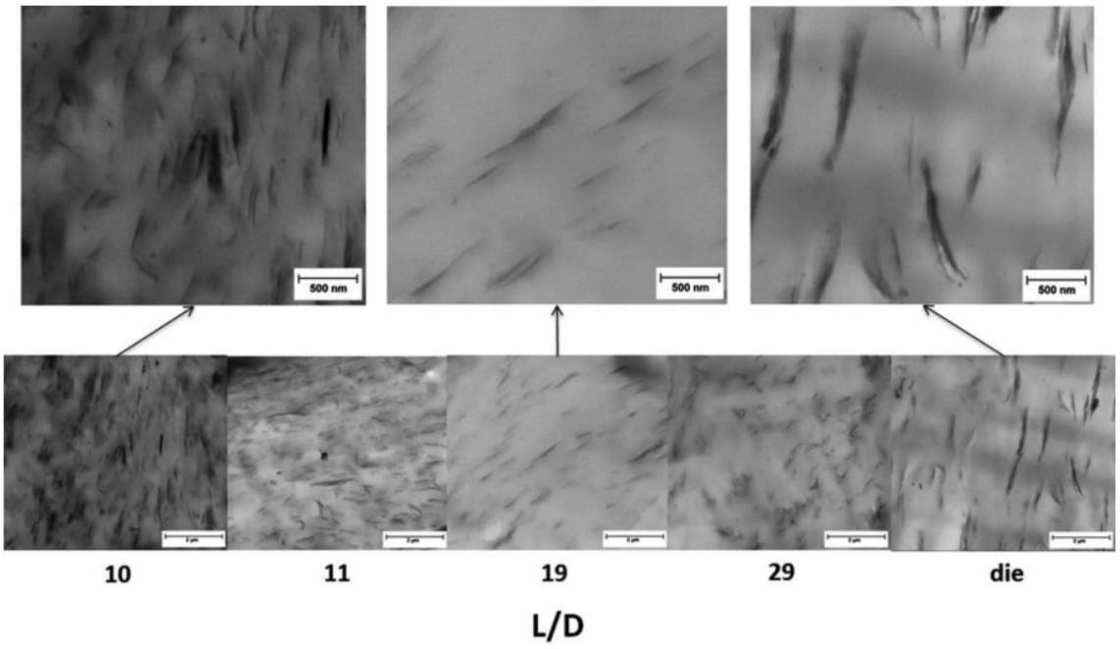

Figure 5. STEM micrographs of the samples collected along the extruder (100rpm, 3 kg h^{-1}).

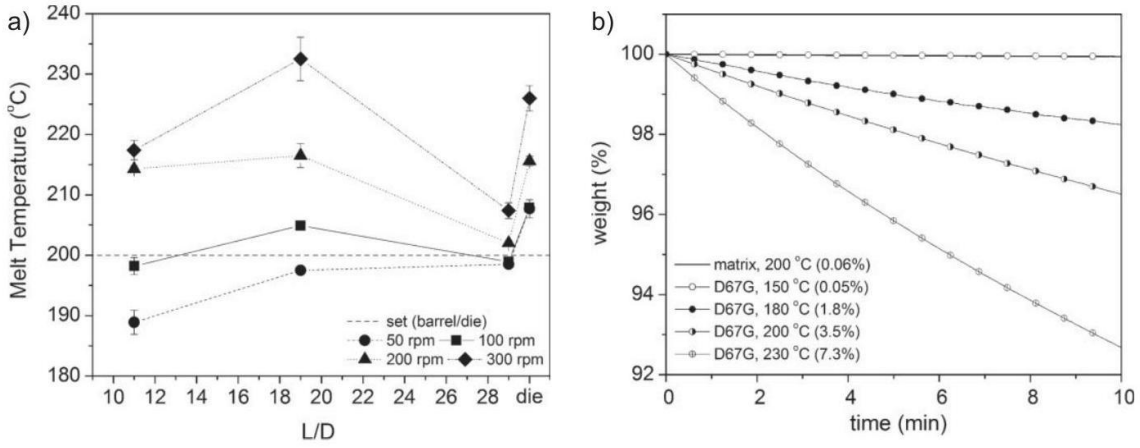

Figure 6. (a) Effect of screw speed on average mass temperature along the extruder; (b) isothermal TGA curves at different temperatures of Dellite 67G.

As demonstrated in Fig. 6b, at temperatures above 180°C the weight loss is substantial due to degradation of the surfactant. This phenomenon should grow in importance with increasing screw speed. Degradation of the clay surfactant reduces clay-polymer affinity. Together with the decrease in melt viscosity caused by viscous dissipation, it facilitates diffusion of the polymer chains out of the clay galleries. Moreover, degradation of the clay surfactant could trigger degradation of the polymer matrix by chain scission. In all, from a rheological point of view, this could entail a decrease of the rheological moduli and of yield stress, as seen in Fig. 3. NIR predictions should also be affected by this decrease, since σ_0 is a major parameter of the chemometric model. The diffusion process cited above could eventually cause the collapse of the clay galleries, as seen in the STEM micrograph of the sample collected at the die (Fig. 5) and suggested by various authors [16,18]. It has also been proposed that degradation of the polymer matrix by chain scission changes the hydrodynamic stress balance, the intrinsic attractive forces of the clay platelets becoming dominant and promoting reaggregation of intercalated platelets [5, 28, 32]. However, in the present case, surfactant degradation should be the major cause for the rheological changes.

Effect of Feed Rate on the Evolution of Dispersion

Figs. 7 a and b demonstrate the effect of feed rate on the evolution of dispersion along the extruder axis, using inline NIR and rheometry (melt yield stress, σ_0). Similarly to what was observed for the effect of screw speed, dispersion levels are already substantial at $L/D = 10$ (between 42% and 88%) and increase sharply until $L/D = 11$ (to 86% and 96%, respectively). At this location, the relative values of yield stress - used here as a measure of exfoliation - are near their maximum and already discriminate well the effect of the feed rate. Curiously, at the same location, NIR data shows a positive influence of the feed rate on dispersion which changes downstream. These results confirm the quick development of dispersion, concurrently with matrix melting. From $L/D = 11$ onwards, a distinct evolution pattern sets in, as seen in Figs. 7 c and d , which represent the data normalized to the value at $L/D = 11$. For the lower feed rates, dispersion progresses somewhat until $L/D = 19$, but declines downstream; for the higher feed rates, a continuous reduction takes place. Again, a negative die effect is perceived. As before, XRD and STEM results (Figs. 4 and 5) confirm these observations.

Moreover, as illustrated in Figs. 8 a and b , the normalized values of the FT-IR peak shifts distinguish the contributions of intercalation and exfoliation to dispersion, respectively. As the individual clay layers become more spaced, the peaks at 1050 cm^{-1} and 1080 cm^{-1} tend to shift. When the structure is ordered and intercalated, the peak at 1050 cm^{-1} moves towards a lower wavenumber, whilst for highly disordered or partially exfoliated morphologies the peak at 1080 cm^{-1} shifts to higher wavenumbers [23-24]. Fig. 8 a suggests reversion of intercalation along the extruder and die, particularly in the second part of the screw and for the highest feed rates. Contrariwise, no noteworthy axial changes in exfoliation are detected, maybe with the exception of the die. These results should be considered cautiously, given the small sample volumes analyzed bearing in mind the probable heterogeneity of the samples, particularly upstream, as well as the previous lack of sensitivity revealed by this technique when studying the effect of screw speed.

Fig. 9 displays the recorded evolution of melt temperature along the extruder axis and die (Tab. 2 contains identical data), as well as the minimum residence time at the end of the first mixing zone ($L/D = 11$) and at the die exit. Until $L/D = 11$ and, to a lesser extent, until $L/D = 19$, higher feed rates slow down the temperature development because of the greater volume/surface ratio of material in the partially filled channels and the lower local residence time for heat transfer. There is also a significant decrease of the SME values (Tab. 2), particularly for feed rates higher than 3 kg h^{-1}. Viscous dissipation effects during these experiments were much lower than those caused by increasing screw speed. Mild shearing conditions and enough time are generally required for diffusion of the polymer inside the confined spaces between clay lamella which are already expanded as a result of a chemical treatment [10]. At this processing stage, the lower the feed rate, the closer the material will be subjected to these best conditions, because a

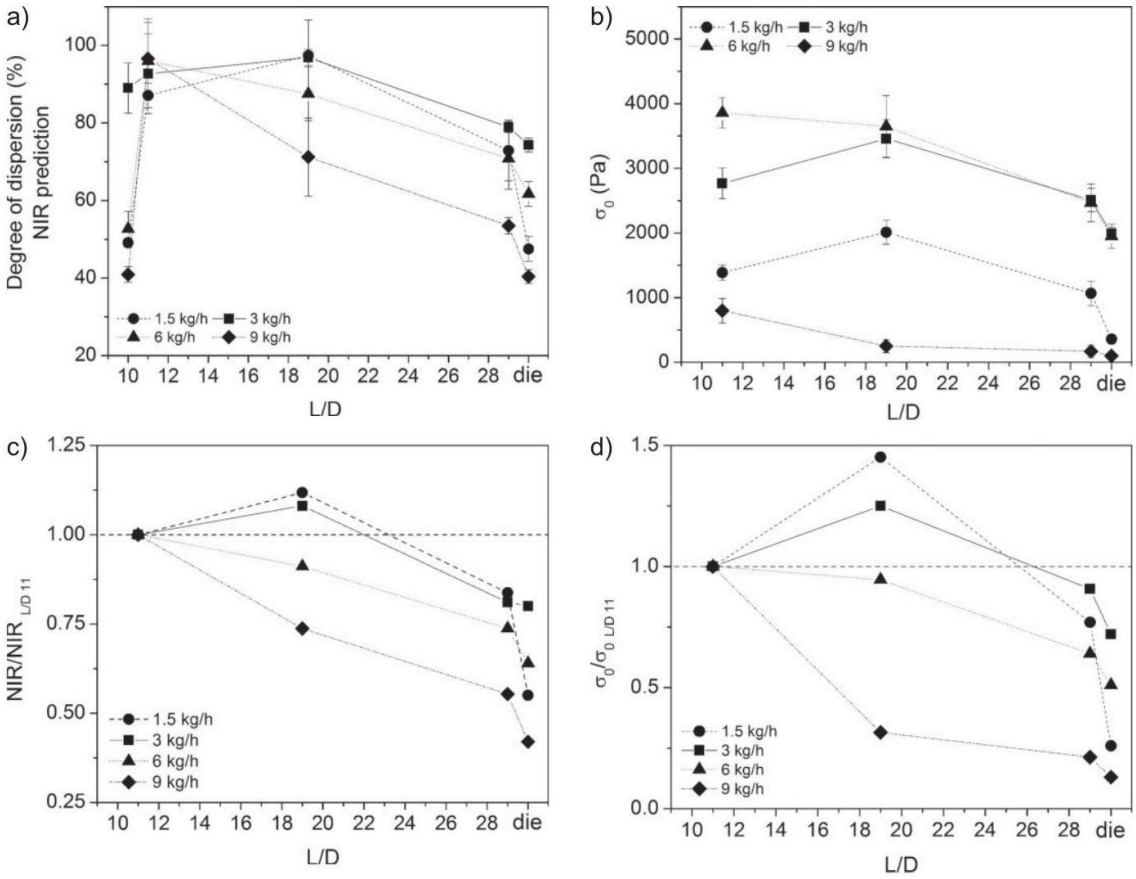

Figure 7. Effect of feed rate on the evolution of dispersion along the extruder axis of PP/clay nanocomposites, as determined by: (a) inline NIR, (b) melt yield stress; (c) and (d) show same data normalized to the values measured at $L/D = 11$.

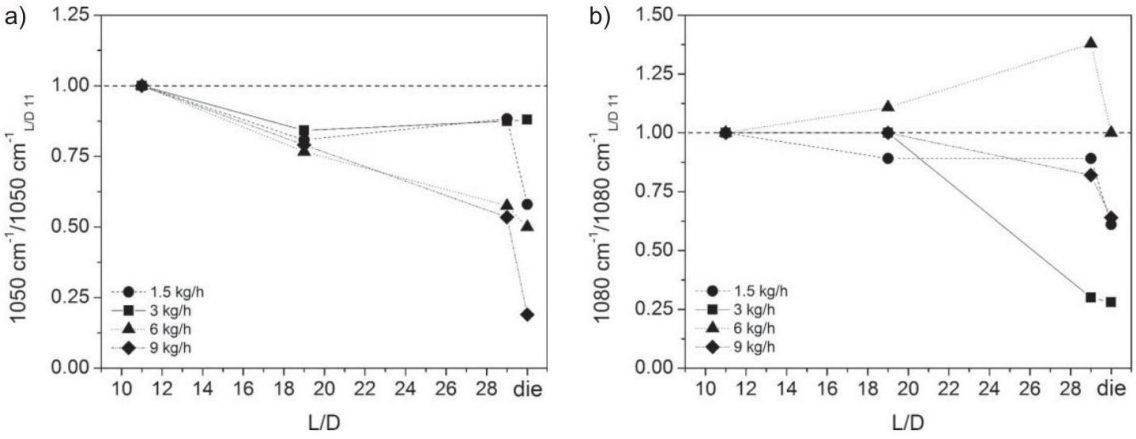

Figure 8. Effect of feed rate on the normalized FT-IR peak shifts along the extruder: (a) in-plane peak at 1050 cm^{-1}; (b) out-of-plane peak at 1080 cm^{-1}.

higher temperature is associated to a lower viscosity and local residence times will also be higher. A high level of shearing applied after this period of diffusion leads to a high level of exfoliation [10]. Given the interplay between intercalation and exfoliation, it makes

sense that until $L/D = 19$ the levels of both show identical dependency of the feed rate. From $L/D = 19$ onwards, the melt temperature relaxes until the die inlet, because the screws contain only conveying elements (Fig.1). Simultaneously, Fig. 8b clearly indicates that the cumulative residence times reduce drastically with increasing feed rate. Consequently, reversion of intercalation or de-intercalation for the nanocomposites manufactured at the highest feed rates could be associated with relaxation phenomena.

Although the melt temperature drop induces a viscosity increase, the hydrodynamic stress levels should decline because flow is mostly developing in partially filled conveying ele-

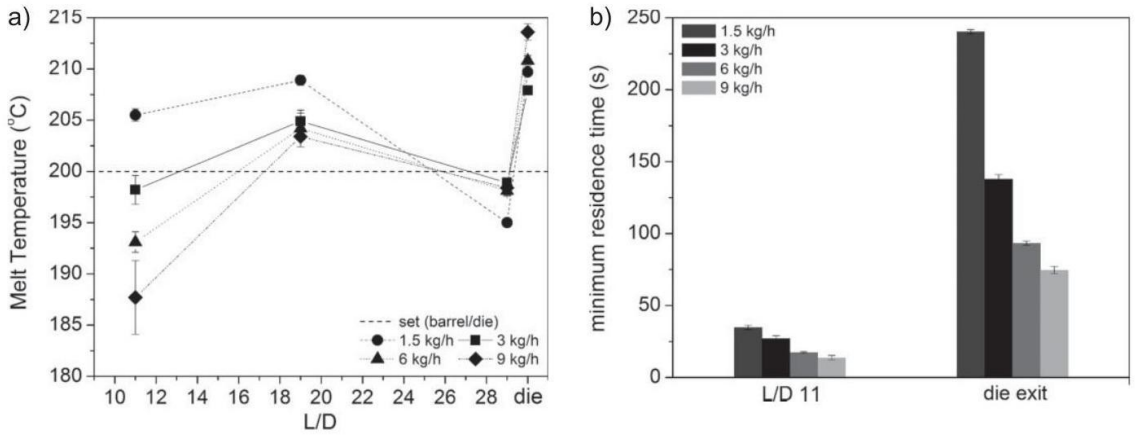

Figure 9. (a) Effect of feed rate on average mass temperature along the extruder; (b) minimum residence time at $L/D = 11$ (end of first mixing zone) and die exit.

ments. Also, these stresses are applied during smaller periods as higher feed rates are used. Henceforth, these conditions could set the stage for partial recovery of the previous deformation, i.e., the melt could partially drain out of the clay galleries. De-intercalation has been addressed as justification for morphology changes in rubber matrix nanocomposites upon vulcanization [33-35] and attributed to the increase of elasticity and viscosity resulting from matrix crosslinking. According to the authors, as long as the processing temperature is above the glass transition temperature of the matrix, without proper mechanical shear relaxation motion of the polymer chains dominates molecular thermodynamics and the intercalated chains can be pulled out of the clay galleries, causing reversal of intercalation [34,35]. This thermodynamic instability of polymer-clay structures above the glass transition temperature has also been proposed by Krishnamoorti et al. [28,32]

Conclusions

Although the preparation of PP-organoclay nanocomposites using co-rotating twin-screw extruders can yield well-dispersed systems, not only screw speed and feed rate are important processing parameters, but the actual evolution of dispersion along the screw axis is far from gradual. Substantial dispersion levels are achieved in the first part of the extruder within a few axial centimeters, simultaneously with melting of the polymer matrix. Apparently, flow along these restrictive screw elements generates the stresses and residence time levels required for a good development of both intercalation and exfoliation. From then onwards, evolution will either develop much slower, remain

basically constant, or reversion may be observed, depending on the processing conditions selected. In all cases, flow along the die seems to have a negative effect on dispersion. Such a complex development was coherently inferred from data obtained by the usual techniques utilized to assess dispersion, namely NIR, rheology, and X-ray diffraction, making use of well-established correlations previously proposed in the literature, as well as transmission electron microscopy. FT-IR spectra were also examined, but the technique ex-
hibited some sensitivity limitations which could be explained by the small volume of sample analyzed.

Reversion of dispersion with increasing screw speed seems to be induced by the parallel growth of viscous dissipation and resultant degradation of the clay surfactant. The latter reduces clay-polymer affinity and, together with the decrease in melt viscosity caused by viscous dissipation, enables diffusion of the polymer chains out of the clay galleries. Degradation of the clay surfactant could also prompt degradation of the polymer matrix by chain scission, with a further decrease in viscosity. Reversion of dispersion with increasing feed rate was related to relaxation phenomena. In the second part of the extruder, the hydrodynamic stress levels should drop due to flow in partially filled screw elements and are exerted during shorter periods. This could enable partial recovery of the previous deformation, with partial drain out of the melt from the clay galleries.

The authors have declared no conflict of interest.

Symbols used

a	[-]	Yasuda parameter
b	[-]	power-law exponent
d_{001}	[nm]	lamellar distance
D	[m]	screw diameter
G'	[Pa]	storage modulus
G''	[Pa]	loss modulus
L	[m]	axial length of extruder
MFI	[g 10 min^{-1}]	melt flow index
N	[rpm]	screw speed
Q	[kgh^{-1}]	feed rate
SD	[-]	standard deviation
SME	[kWht^{-1}]	specific mechanical energy

Greek symbols

η^*	[Pa s]	complex viscosity
η_0	[Pa s]	viscosity at zero shear
θ	[°]	angle

λ	[Å]	wavelength
σ_0	[Pa]	melt yield stress
τ	[s]	relaxation time
ω	[rads^{-1}]	angular frequency

References

[1] J. W. Cho, D. R. Paul, Polymer 2001, 42 (3), 1083-1094. DOI: 10.1016/S0032-3861 (00)00380-3
[2] H. R. Dennis, D. L. Hunter, D. Chang, S. Kim, J. L. White, J. W. Cho, D. R. Paul, Polymer 2001, 42 (23), 9513-9522. DOI: 10.1016/S0032-3861(01)00473-6
[3] W. Lertwimolnun, B. Vergnes, Polym. Eng. Sci. 2007, 47 (12), 2100-2109. DOI: 10.1002/pen. 20934
[4] S. Tanoue, L. A. Utracki, A. Garcia-Rejon, J. Tatibouet, K. C. Cole, M. R. Kamal, Polym. Eng. Sci. 2004, 44 (6), 1046-1060. DOI: 10.1002/pen. 20098
[5] L. Xu, H. Nakajima, E. Manias, R. Krishnamoorti, Macromolecules 2009, 42 (11), 3795-3803. DOI: 10.1021/ma9002853
[6] M. W. Spencer, L. Cui, Y. Yoo, D. R. Paul, Polymer 2010, 51 (5), 1056-1070. DOI: 10.1016/j.polymer.2009.12.047
[7] K. Chrissopoulou, S. H. Anastasiadis, Eur. Polym. J. 2011, 47 (4), 600-613. DOI: 10.1016/j.eurpolymj.2010.09.028
[8] L. Zhu, M. Xanthos, J. Appl. Polym. Sci. 2004, 93 (4), 18911899. DOI: 10.1002/app. 20658
[9] W. Lertwimolnun, B. Vergnes, Polym. Eng. Sci. 2006, 46 (3), 314-323. DOI: 10.1002/pen. 20458
[10] M. Bousmina, Macromolecules 2006, 39 (12), 4259-4263. DOI: 10.1021/ma052647f
[11] B. Lin, A. Thümen, H.-P. Heim, G. Scheel, U. Sundararaj, Polym. Eng. Sci. 2009, 49 (4), 824-834. DOI: 10.1002/ pen. 21327
[12] T. Domenech, E. Peuvrel-Disdier, B. Vergnes, Int. Polym. Process. 2012, 27 (5), 517-526. DOI: 10.3139/217.2591
[13] P. D. Fasulo, W. R. Rodgers, R. A. Ottaviani, D. L. Hunter, Polym. Eng. Sci. 2004, 44 (6), 1036-1045. DOI: 10.1002/ pen. 20097
[14] L. Scatteia, P. Scarfato, D. Acierno, e-Polymers 2006, 23, 1-15.
[15] A. L. F. Giraldi, M. T. M. Bizarria, A. A. Silva, J. I. Velasco, M. A. d'Ávila, L. H. I. Mei, J. Appl. Polym. Sci. 2008, 108 (4), 2252-2259. DOI: 10.1002/app. 27280
[16] R. K. Shah, D. R. Paul, Polymer 2006, 47 (11), 4075-4084. DOI: 10.1016/j.polymer.2006.02.031
[17] J. M. Barbas, A. V. Machado, J. A. Covas, Chem. Eng. Sci. 2013, 98, 77-87. DOI: 10.1016/j.ces.2013.05.004
[18] N. Nassar, L. A. Utracki, M. R. Kamal, Int. Polym. Process. 2005, 20 (4), 423-431.

[19] W. Xie, Z. Gao, W. Pan, D. Hunter, A. Singh, R. Vaia, Chem. Mater. 2001, 13 (9), 2979-2990. DOI: 10.1021/cm010305s
[20] J. M. Barbas, A. V. Machado, J. A. Covas, Polym. Test. 2012, 31 (4), 527-536. DOI: 10.1016/j.polymertesting.2012.02.005
[21] J. M. Barbas, A. V. Machado, J. A. Covas, J. Appl. Polym. Sci. 2013, 127 (6), 4899-4909. DOI: 10.1002/app. 38106
[22] A. V. Machado, J. A. Covas, M. van Duin, J. Appl. Polym. Sci. 1999, 71 (1), 135-141. DOI: 10.1002/(SICI)1097-4628 (19990103)71:1<135::AID-APP16>3.0.CO;2-M
[23] K. C. Cole, Macromolecules 2008, 41 (3), 834-843. DOI: 10.1021/ma0628329
[24] W. L. IJdo, S. Kemnetz, D. Benderly, Polym. Eng. Sci. 2006, 46 (8), 1031-1039. DOI: 10.1002/pen. 20523
[25] A. Durmus, A. Kasgoz, C. W. Macosko, Polymer 2007, 48 (15), 4492-4502. DOI: 10.1016/j.polymer.2007.05.074
[26] A. Vermogen, K. Masenelli-Varlot, R. Séguéla, J. Duchet-Rumeau, S. Boucard, P. Prele, Macromolecules 2005, 38 (23), 9661-9669. DOI: 10.1021/ma051249+
[27] P. Cassagnau, Polymer 2008, 49 (9), 2183-2196. DOI: 10.1016/j.polymer.2007.12.035
[28] R. Krishnamoorti, E. P. Giannelis, Macromolecules 1997, 30 (14), 4097-4102. DOI: 10.1021/ma960550a
[29] D. Kim, J. S. Lee, C. F. Barry, J. L. Mead, J. Appl. Polym. Sci. 2008, 109 (5), 2924-2934. DOI: 10.1002/app. 28394
[30] I. Manas-Zloczower, D. L. Feke, in Mixing and Compounding of Polymers: Theory and Practice (Ed: I. Manas-Zloczower), Carl Hanser Verlag, Munich 2009.
[31] V. Yquel, A. V. Machado, J. A. Covas, J. J. Flat, J. Appl. Polym. Sci. 2009, 114 (3), 1768-1776. DOI: 10.1002/app. 30680
[32] J. Ren, B. F. Casanueva, C. A. Mitchel, R. Krishnamoorti, Macromolecules 2003, 36 (11), 4188-4194. DOI: 10.1021/ ma025703a
[33] K. G. Gatos, J. Karger-Kocsis, Polymer 2005, 46 (9), 30693076. DOI: 10.1016/j.polymer.2005.01.095
[34] X. Wang, A. Huang, D. Jia, Y. Li, Eur. Polym. J. 2008, 44 (9), 2784-2789. DOI: 10.1016/j.eurpolymj.2008.06.035
[35] L. Sun, E. A. Ertel, L. Zhu, B. S. Hsiao, C. Avila-Orta, I. Sics, Langmuir 2005, 21 (13), 5672-5676. DOI: 10.1021/la047087c